

CAV2009 – Paper No. 172

SHOCK PROPAGATION IN POLYDISPERSE BUBBLY FLOWS

Keita Ando* **Tim Colonius**

Christopher E. Brennen

Division of Engineering and Applied Science

California Institute of Technology

Pasadena, CA 91125

Email: kando@caltech.edu

ABSTRACT

The effect of distributed bubble nuclei sizes on shock propagation in dilute bubbly liquids is computed using a continuum two-phase model. An ensemble-averaging technique is employed to derive the statistically averaged equations and a finite-volume method is used to solve the model equations. The bubble dynamics are incorporated using a Rayleigh-Plesset-type equation which includes the effects of heat transfer, liquid viscosity and compressibility. The numerical model is verified by computing linear wave propagation and comparing to the acoustic theory of dilute bubbly liquids. It is known that for the case of monodisperse mixtures, relaxation oscillations occur behind the shock due to the bubble dynamics. The present computations show that bubble size distributions lead to additional damping of the average shock dynamics. If the distribution is sufficiently broad, the effect of polydispersity dominates over the single-bubble-dynamic damping and the shock profile is smoothed out. The size distribution effect on bubble screen problems is also discussed.

INTRODUCTION

A fundamental understanding of the dynamics of bubbly flows is of great importance in underwater explosions [1, 2], a spallation neutron source [3, 4], turbomachinery [5–7] and shock wave lithotripsy [8–10]. In such flows, cavitation frequently occurs due to tension in the liquid phase. Shock dynamics provide a canonical example where cavitation and bubble dynamics have

a large effect on the shock structure and propagation speed. Most of the previous studies [11–19] have focused on shock propagation in monodisperse bubbly liquids (i.e. all the bubbles initially have the same size.). However, in flows of practical interest, the nuclei size is broadly distributed; thus, the size distributions need to be included for more realistic modeling. We treat the liquid and disperse phases as a continuum medium and solve statistically averaged equations to determine the average shock structure.

First, we present the continuum and bubble-dynamic models with their assumptions and discuss the model limitations. Next, we formulate and verify the numerical scheme developed to solve the system. Then, we solve one-dimensional wave propagation in dilute bubbly liquids with bubble size distributions (i.e. polydisperse mixtures) and describe the effects of the size distributions on linear and nonlinear wave propagation. We also conduct parameter studies of probable bubble sizes, void fractions and shock strengths to investigate the effects of these parameters on shock structure. Finally, we examine shock propagation through polydisperse bubble screens.

MODEL EQUATIONS

Continuum model

We use an ensemble-averaging technique [20, 21] to derive the averaged mixture equations. The mixture model assumes that (a) the bubbles are spherical; (b) mutual interactions among the bubbles are negligible except through their effect on the mixture-averaged flow; (c) wavelengths in the mixture are large compared

*Address all correspondence to this author.

to the mean bubble spacing; (d) the bubbles advect with the ambient liquid velocity (no slip); and (e) density and velocity fluctuations in the liquid phase are uncorrelated.

Assumption (a) implies that fission and coalescence of the bubbles are not permitted, so that the bubble number is conserved in time. Assumptions (b) to (d) are generally valid in the dilute limit, which is used for the model closure. Relative motion between the phases has been shown to have minimal impact on linear wave propagation [22] and also plays a minor role in shock propagation [18]. Assumption (e) is reasonable due to the fact that the velocity fluctuations caused by the bubble dynamics concentrate in the vicinity of the bubbles, where the liquid is effectively incompressible [23].

Under these assumptions, we may write the one-dimensional conservation equations (mass, momentum and bubble number conservation) as

$$\frac{\partial \rho}{\partial t} + \frac{\partial \rho u}{\partial x} = 0, \quad (1)$$

$$\frac{\partial \rho u}{\partial t} + \frac{\partial}{\partial x} (\rho u^2 + p_l) = \frac{\partial \tilde{p}}{\partial x}, \quad (2)$$

$$\frac{\partial n}{\partial t} + \frac{\partial n u}{\partial x} = 0. \quad (3)$$

Here, u is velocity, n is bubble number per unit volume of the mixture and ρ is mixture density approximated by $(1 - \alpha)\rho_l$ where ρ_l is liquid density and α is void fraction, and p_l is liquid pressure described by the Tait equation of state (EOS) [24],

$$\frac{p_l + B}{p_{l0} + B} = \left(\frac{\rho_l}{\rho_{l0}} \right)^\gamma = \frac{1}{\rho_{l0}^\gamma} \left(\frac{\rho}{1 - \alpha} \right)^\gamma, \quad (4)$$

where ρ_{l0} is reference liquid density at ambient pressure, p_{l0} , and γ and B stand for stiffness and tensile strength of the liquid, respectively. The value of B is usually set constant, so that the Tait EOS (4) describes the homentropic behavior of the liquid phase. For water, we take $\gamma = 7.15$ and $B \approx 3000$ atm. The term, \tilde{p} , on the right-hand side of momentum equation (2) represents pressure fluctuations due to the phase interactions [25],

$$\tilde{p} = \alpha \left(p_l - \frac{\overline{R^3 p_{bw}}}{\overline{R^3}} - \rho \frac{\overline{R^3 \dot{R}^2}}{\overline{R^3}} \right), \quad (5)$$

where R is bubble radius, \dot{R} is bubble wall velocity and p_{bw} is bubble wall pressure described by the dynamic boundary condition [7],

$$p_{bw} = p_b - 4\mu_l \frac{\dot{R}}{R} - \frac{2S}{R}. \quad (6)$$

Here, p_b is internal bubble pressure (sum of vapor pressure, p_v , and noncondensable gas pressure, p_g), μ_l is liquid viscosity and S is surface tension. The overbars in equation (5) denote moments with respect to the (normalized) bubble size distributions, $f(R_0)$,

$$\overline{\phi}(x, t) = \int_0^\infty \phi(x, t; R_0) f(R_0) dR_0, \quad (7)$$

where R_0 is equilibrium bubble radius corresponding to the ambient pressure and ϕ represents any of R^3 , $R^3 p_{bw}$ or $R^3 \dot{R}^2$. The void fraction is then defined as

$$\alpha = \frac{4\pi}{3} n \overline{R^3}. \quad (8)$$

Note the functional dependence of R_0 on the size distribution is assumed spatially uniform. This assumption is valid for all times due to the no-slip assumption (d). Also note that equation (7) implies that the bubble dynamics in the neighborhood of x coincide if the equilibrium radius is the same. This implication is consistent with the assumption (c).

It should be noted that the term, \tilde{p} , in momentum equation (2) does not appear in van Wijngaarden's volume-averaged equations [26]. For linearized dynamics of the spherical bubbles, \tilde{p} contains corrections of order at most $O(\alpha^2)$, so that the ensemble-averaged equations (1) to (3) reduce to van Wijngaarden's equations in the linear context.

In this paper, we model the size distribution using a lognormal function with standard deviation, σ ,

$$f(R_0^*) = \frac{1}{\sqrt{2\pi}\sigma R_0^*} \exp \left(-\frac{\ln^2 R_0^*}{2\sigma^2} \right), \quad (9)$$

where $R_0^* = R_0/R_0^{\text{ref}}$ (R_0^{ref} represents the probable size.). The lognormal function (9) approaches zero exponentially in the limit of $\ln R_0^* \rightarrow \infty$, so that contributions of extremely large sizes, which may deteriorate the continuum model accuracy, to integration (7) can be minimized. In the limit of $\sigma \rightarrow 0$, the lognormal function (9) reduces to the Dirac delta function,

$$f(R_0^*) = \delta(R_0^* - 1), \quad (10)$$

which models monodisperse mixtures.

Figure 1 shows the measured size distributions in a water tunnel [27] and the ocean [28], together with the lognormal function (9). It follows that $\sigma = 0.7$ may be a reasonable value to model the actual distributions in engineering flows and ocean, but we use the distribution (9) as illustrative of the qualitative effects of polydispersity rather than to model a particular system.

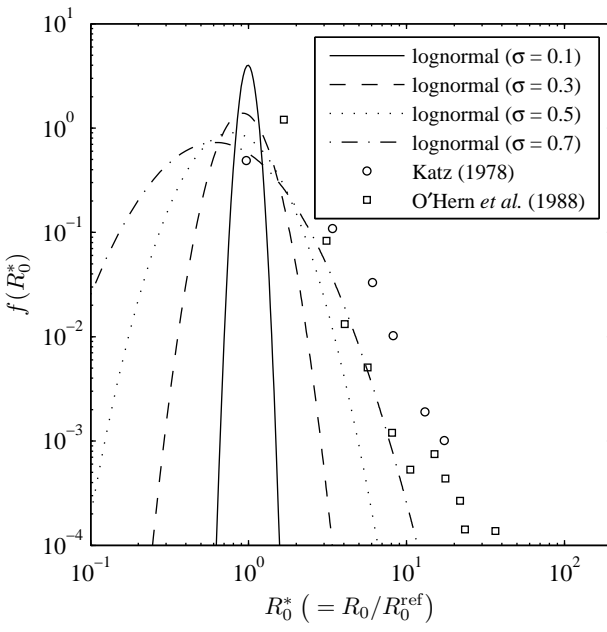


Figure 1. Normalized size distributions of equilibrium bubble radius. Lines denote the lognormal function (9) with standard deviation, σ . The probable size, R_0^{ref} , is set to be $10\mu\text{m}$.

Bubble-dynamic model

In order to accurately resolve the bubble dynamics, the detailed conservation equations of both phases need to be solved, but such a computation is prohibitive. This necessitates introducing the following simplifications.

The spherical-bubble-dynamic model assumes that (f) the bubble contents (noncondensable gas and vapor) have spatially uniform pressure; (g) the bubble contents are perfect; (h) the liquid is cold (far from the boiling point); (i) the mass of noncondensable gas in the bubble is unchanged; and (j) phase change occurs instantaneously.

The homobaric assumption (f) is valid since the inertia of the bubble contents is negligible compared to that of the liquid. The cold liquid assumption (h) leads to undisturbed liquid temperature at the bubble wall, so that the energy equation in the liquid phase is unnecessary to solve [29, 30]. The typical bubble growth rate due to mass transfer of dissolved air in water is so slow (compared to the bubble oscillation rate) that assumption (i) is reasonable [31]. Assumptions (h) and (j) imply constant vapor pressure at the bubble wall, which is typically adequate except near the end of a violent bubble collapse [32].

The Gilmore equation [33],

$$R\ddot{R}\left(1-\frac{\dot{R}}{C}\right)+\frac{3}{2}\dot{R}^2\left(1-\frac{\dot{R}}{3C}\right)=H\left(1+\frac{\dot{R}}{C}\right)+\frac{RH}{C}\left(1-\frac{\dot{R}}{C}\right), \quad (11)$$

is used to evaluate the spherical bubble dynamics (H and C are enthalpy and sonic speed, respectively, at the bubble wall in the liquid; the dots denote the substantial time derivative). The rate of the bubble energy change equals the sum of work done by the bubble wall and energy transferred due to the mass flux of vapor and the heat flux at the bubble wall. That is,

$$\begin{aligned} & \frac{d}{dt} \int_0^{R(t)} (\rho_g e_g + \rho_v e_v) 4\pi \xi^2 d\xi \\ &= 4\pi R^2 \left(-\dot{R} p_b + c_{pv} T_w \dot{m}_v'' + k_{bw} \frac{\partial T}{\partial r} \Big|_w \right), \end{aligned} \quad (12)$$

where subscripts g , v , b and w denote noncondensable gas, vapor, bubble contents (gas/vapor mixture) and bubble wall properties, respectively, ρ is density, e is internal energy, c_p is specific heat at constant pressure, T_w is (undisturbed) bubble wall temperature, \dot{m}'' is mass flux, k is thermal conductivity, T is temperature (defined inside the bubble) and r is a radial coordinate measured from the bubble center. With assumptions (f) and (g), the energy balance (12) reduces to the following equation [29, 34],

$$\dot{p}_b = \frac{3\gamma_b}{R} \left(-\dot{R} p_b + \mathcal{R}_v T_w \dot{m}_v'' + \frac{\gamma_b - 1}{\gamma_b} k_{bw} \frac{\partial T}{\partial r} \Big|_w \right), \quad (13)$$

where γ_b is specific-heat ratio of the bubble contents and \mathcal{R}_v is the gas constant of vapor. In the derivation, it is assumed that the specific ratio of noncondensable gas, γ_g , is nearly the same as that of vapor, γ_v , so that $\gamma_b \approx \gamma_g \approx \gamma_v$. In equation (13), vapor flux and heat conduction at the bubble wall are estimated using the reduced-order model of Preston *et al.* [30], which is found to be accurate for bubbles of small Peclet numbers (i.e. small-sized bubbles). The detailed system of the bubble-dynamic equations is found in [30, 35].

Model limitations

We now discuss specific limitations associated with assumptions (a) and (b), which are essential for deriving the continuum model (1) to (3).

The spherical-bubble assumption (a) implies no fission of the bubbles; the bubble number conservation (3) is then formulated. Possible mechanisms responsible for the bubble fission

are a re-entrant jet and a Rayleigh-Taylor-type instability [36]. If the thickness of the incident shock is comparable to or smaller than the bubble sizes, the bubbles distort nonspherically and may finally result in fission due to the re-entrant jet. However, the interaction of the averaged pressure field and the bubble cloud is known to broaden the shock thickness. As a result, the bubble fission does not occur frequently if the shock strength is sufficiently small [15]. For very strong shocks, the bubble collapse is so violent that nonspherical distortions may arise due to the spherical equivalent of the Rayleigh-Taylor instability and the fission may occur.

To validate assumption (b), the mean bubble spacing, $l = n^{-1/3}$, must be much larger than the bubble sizes. It follows from equation (8) that this condition is satisfied in the dilute limit (i.e. $\alpha \rightarrow 0$). The acoustic theory of linear waves in monodisperse bubbly liquids [37, 38] is known to overestimate attenuation under the resonant condition since the bubble/bubble interactions can never be ignored even in the dilute limit [38, 39]. Inclusion of the broad size distribution (e.g. large standard deviation, σ , in lognormal distribution (9)) can deemphasize errors associated with resonance since the probability that a bubble of certain size, R_0 , is under resonance is low among a broad spectrum of R_0 [40].

NUMERICAL METHOD

The system of equations thus consists of the ensemble-averaged equations (1) to (3) and the bubble-dynamic equations (11) and (13) in a conservation form. In the absence of the source terms, the system is hyperbolic; a shock capturing scheme is chosen. A third-order TVD Runge-Kutta scheme [41] marches the system forward in time. The spatial discretization is handled by a fifth-order finite-volume WENO scheme [42] coupled with an HLLC approximate Riemann solver [43]. The WENO reconstruction is performed in characteristic space. The numerical quadrature of (7) is evaluated using Simpson's rule; 401 quadrature points are used for bubble screen computation, but otherwise 101 quadrature points are used. The computational grid is uniform with cell width, $\Delta x = R_0^{\text{ref}}$. The maximum CFL number is set to be 0.1, which is small enough to resolve the bubble dynamics associated with the small bubbles with $R_0 < R_0^{\text{ref}}$ in polydisperse cases.

Nonreflecting boundary conditions [44] are implemented to minimize spurious, incoming waves. Outgoing waves are evaluated using a fourth-order one-sided difference scheme. The sonic speed of bubbly liquids in the quasistatic limit (polytropic index of the noncondensable gas, $\kappa \rightarrow 1$ [45, 46]),

$$c = \sqrt{\frac{\gamma(p_l + B)}{\rho} \frac{\kappa p_l}{\alpha\gamma(p_l + B) + (1 - \alpha)\kappa p_l}}, \quad (14)$$

is used at boundaries [7]. Note that in the dilute limit, c reduces

to the sonic speed of the liquid alone.

One issue in computing polydisperse cases in characteristic space is that the transformation matrix to compute the characteristic variables is not sparse and the transformation is computationally expensive. To avoid evaluating such a dense matrix, we rewrite the bubble number conservation (3) in terms of void fraction:

$$\frac{\partial \alpha}{\partial t} + \frac{\partial \alpha u}{\partial x} = 3\alpha \frac{\overline{R^2 R}}{\overline{R^3}}. \quad (15)$$

Given the void fraction, the bubble number density is computed by

$$n = \sqrt{\frac{4\pi}{3\alpha} \int_0^\infty (nR)^3 f(R_0) dR_0}. \quad (16)$$

Another issue may arise in bubble screen problems that consist of pure liquid and bubble cloud domains. A void fraction in the pure liquid domain is conceptually zero, but the zero void fraction is numerically undesirable since numerical oscillations that possibly occur in the neighborhood of the liquid/bubble-cloud interface give rise to negative void fractions. One possible way to avoid this is to add a tiny void fraction in the liquid domain. Provided that the void fraction is sufficiently small (say, $\alpha = 10^{-7}$), the wave propagation can be considered essentially nondispersivve.

LINEAR WAVE PROPAGATION

Dispersive wave structure

We consider one-dimensional linear wave propagation in an air/water mixture of $\alpha_0 = 0.1\%$ at standard temperature and pressure (STP: $T_0 = 20^\circ\text{C}$, $p_{l0} = 1\text{ atm}$). The bubble size is assumed lognormally distributed about $R_0^{\text{ref}} = 10\mu\text{m}$ with $\sigma = 0$ (monodisperse) and $\sigma = 0.7$ (polydisperse). For simplicity, vapor flux, \dot{m}_v'' , in equation (13) is ignored since vapor pressure is small compared to the ambient pressure. We initially ($t = 0$) impose a Gaussian perturbation in liquid pressure,

$$p_l(x) = p_{l0} + \Delta p_l \exp \left[- \left(\frac{x - x_0}{h} \right)^2 \right], \quad (17)$$

where $x_0 = 0$, $h = 4R_0^{\text{ref}}$, and perturbation amplitude, Δp_l , is made small (say, $\Delta p_l = 10^{-4}p_{l0}$) in order that nonlinearity in the system of equations be eliminated. All the bubbles are assumed to initially be in equilibrium with perturbed liquid pressure (17). The physical properties are taken from [47].

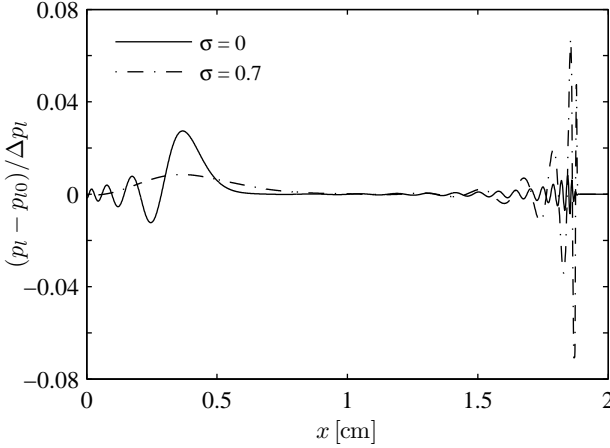


Figure 2. Liquid pressure distribution at $t = 12.7 \mu\text{s}$ for linear wave propagation in an air/water mixture of $\alpha_0 = 0.1\%$ and $R_0^{\text{ref}} = 10 \mu\text{m}$.

The liquid pressure distribution at $t = 12.7 \mu\text{s}$ is shown in figure 2. As observed in the experiment of Kuznetsov *et al.* [48], the waves have an oscillatory structure (relaxation oscillations) that arises due to the bubble dynamics. The high-wavenumber waves seen around $x = 1.8 \text{ cm}$ propagate essentially with the sonic speed of water alone, c_l , and thus correspond to the ultrasonic waves. On the other hand, the low-wavenumber waves seen around $x = 0.5 \text{ cm}$ propagate more slowly than c_l , and therefore are classified in the low-frequency (quasistatic) regime. It should be pointed out that the size distribution smooths out the oscillatory structure in the low-frequency signal. In other words, the size distribution leads to additional damping of the wave propagation.

Bubble statistics

We now examine the statistics of the bubble size distribution. It follows from Prosperetti [45] and Prosperetti *et al.* [29] that the natural frequency of the bubbles is written as

$$\omega_N^2 = \frac{p_{g0}}{\rho_l R_0^2} \left(3\kappa - \frac{2S}{p_{g0}R_0} \right) + \frac{(\omega R_0/c_l)^2}{1 + (\omega R_0/c_l)^2} \omega^2, \quad (18)$$

where p_{g0} is internal bubble pressure given by $p_{l0} - p_v + (2S/R_0)$, ω is temporal angular frequency ($\omega = 2\pi f$) and the last term on the right hand side represents the contribution associated with liquid compressibility. The isothermal natural frequency is obtained in the quasistatic limit (i.e. $\omega \rightarrow 0$):

$$\omega_N^2|_{\kappa=1} = \frac{p_{g0}}{\rho_l R_0^2} \left(3 - \frac{2S}{p_{g0}R_0} \right). \quad (19)$$

As a result, the different-sized bubbles oscillate with different frequencies. On the other hand, under the ultrasonic condition (i.e. $\omega \gg \omega_N|_{\kappa=1}$), $\omega_N \approx \omega$, so that the natural frequency is independent of the bubble size.

To help understand effects of polydispersity, consider a one-way-coupling problem, in which the moments of the distribution of equilibrium radius are defined as

$$\mu_j(x, t) = \int_0^\infty R^j(x, t; R_0) f(R_0) dR_0, \quad (20)$$

where j is an integer. Note that void fraction is proportional to the third moment ($j = 3$). In the particular case where bubble oscillations are excited by an impulsive change in farfield liquid pressure, it has been mathematically shown that (linear and nonlinear) inviscid bubble oscillations reach a stationary statistical equilibrium, in which phase cancellations among the different-sized bubbles lead to time-invariant values of the moments [35]. That is, at the statistical equilibrium where the different-sized bubbles oscillate totally out of phase, the polydisperse bubble cloud locally in the neighborhood of x can be considered stationary (or quasistationary if the ambient pressure varies slowly) even though the bubbles keep oscillating. It has also been shown that the statistical equilibrium is achieved rapidly (compared to single-bubble-dynamic damping due to heat conduction, liquid viscosity and compressibility) if the size distribution is sufficiently broad [35, 49].

We revisit the linear wave propagation in figure 2. For the low-frequency waves in the polydisperse case, all the different-sized bubbles oscillate with a phase shift that depends on the bubble size [50]. Thus, phase cancellations due to different phases in the polydisperse bubble cloud occur in the one-way-coupling sense. As a result, the cloud oscillations are damped by this cancellation effect and the oscillatory wave structure, which arises due to dynamics of the monodisperse cloud, is smoothed out. On the other hand, for the ultrasonic (high-frequency) waves, all the different-sized bubbles oscillate with the same phase shift, so that the phase cancellations do not occur [50]. Hence, the wave structure in the polydisperse case is still oscillatory as seen in figure 2.

Dispersion relation

To verify the numerical scheme, the phase velocity and attenuation of the linear wave propagation in figure 2 are computed and compared to the acoustic theory [38], which may be derived by linearizing van Wijngaarden's volume-averaged equations [26]. Since the ensemble-averaged equations (1) to (3) reduce to van Wijngaarden's equations in the linear case, the computed phase velocity and attenuation need to agree with the theoretical values. The phase velocity, V , and attenuation, A (in dB

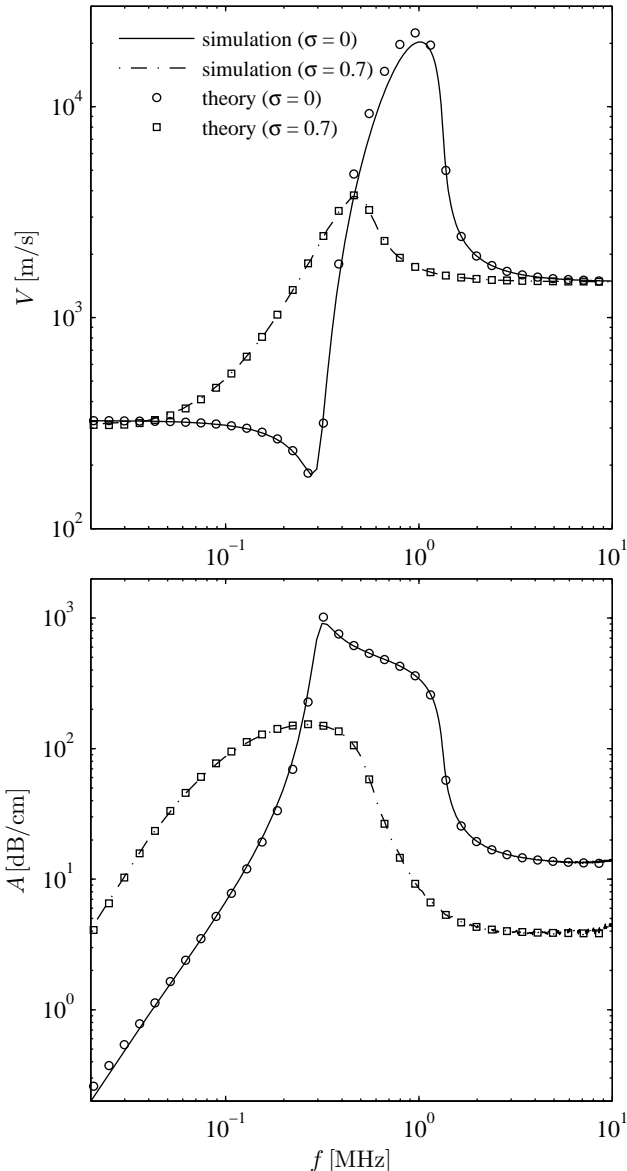


Figure 3. Phase velocity (top) and attenuation (bottom) of linear wave propagation in the air/water mixture in figure 2. The isothermal natural frequency for R_0^{ref} is 0.291 MHz.

per unit length), are defined as

$$V = \left[\Re \left\{ \frac{1}{c_m} \right\} \right]^{-1}, \quad (21)$$

$$A = -20(\log_{10} e) \Im \left\{ \frac{1}{c_m} \right\}, \quad (22)$$

where the complex sonic speed in the mixture, c_m , is given by the dispersion relation [38, 50]. We should note that the effect of liquid compressibility on the natural frequency (18) needs to be retained to accurately evaluate attenuation of ultrasonic waves since the damping due to liquid compressibility dominates over the viscous and thermal contributions for such a high-frequency range [50].

Comparison to the theoretical values (21) and (22) is made in figure 3, where we compute the phase velocity and attenuation by taking a fast Fourier transform (FFT) of the time history of the liquid pressure at two different locations in figure 2. Good agreement in a wide range of frequency totally verifies the numerical scheme. The slight deviations from the theory result from Preston's reduced-order model [30] for evaluating heat conduction at the bubble wall since the model is never exact for finite values of Pe, where the Peclet number is defined as

$$\text{Pe} = \frac{\omega_N|_{\kappa=1} R_0^{\text{ref}2}}{\alpha_T} \propto \left(\frac{R_0^{\text{ref}}}{\delta_T} \right)^2. \quad (23)$$

In this expression, α_T is thermal diffusivity of the bubble contents and δ_T stands for thermal boundary layer thickness at the bubble wall in the case of the linearized bubble dynamics. In this example (10-μm air bubbles at STP), $\text{Pe} = 9.89$. It should be emphasized that Preston's model enables us to avoid solving the detailed conservation equations inside the bubble and therefore dramatically reduces the computational effort.

As described in the preceding section, phase cancellations among the different-sized bubbles in the polydisperse mixture occur in the low-frequency range ($\omega < \omega_N|_{\kappa=1}$) and lead to apparent damping of the linear wave propagation. This explains the fact that the size distribution increases the attenuation for $\omega < \omega_N|_{\kappa=1}$ in figure 3.

SHOCK PROPAGATION

Steady shock relations

We first derive steady shock relations that can be employed as initial conditions to compute shock problems. In front of the shock, the bubbles are in equilibrium with (R_0, T_0, p_{l0}) . Far downstream of the shock front, the bubble dynamics are finally damped and the bubbles are in equilibrium with (R_H, T_0, p_{lH}) where R_H is a new equilibrium radius corresponding to shock pressure, $p_{lH} > p_{l0}$. Note that under the equilibrium state, the source terms in the governing equations vanish. The system (1)

to (3) is written in a frame of the moving shock of speed, U_s :

$$\frac{\partial \rho u'}{\partial x'} = 0, \quad (24)$$

$$\frac{\partial}{\partial x'} (\rho u'^2 + p_l - \tilde{p}) = 0, \quad (25)$$

$$\frac{\partial n u'}{\partial x'} = 0, \quad (26)$$

where the new coordinate system is defined as

$$x' = x - U_s t, \quad u' = u - U_s, \\ \frac{\partial}{\partial x'} = \frac{\partial}{\partial x}, \quad \frac{\partial}{\partial t} = -U_s \frac{\partial}{\partial x}. \quad (27)$$

Integrating equations (24) to (26) from the upstream point (denoted by subscript 0) to the far downstream point (denoted by subscript H), we find

$$-\rho_H u'_H = \rho_0 U_s, \quad (28)$$

$$\rho_H u'_H^2 + p_{lH} = \rho_0 U_s^2 + p_{l0}, \quad (29)$$

$$-n_H u'_H = n_0 U_s, \quad (30)$$

where $\rho_0 = (1 - \alpha_0)\rho_{l0}$ and $\rho_H = (1 - \alpha_H)\rho_{lH}$. The shock pressure, p_{lH} , can be written as

$$p_{lH} = \left(p_{l0} - p_v + \frac{2S}{R_0} \right) \left(\frac{R_H}{R_0} \right)^{-3\kappa} + p_v - \frac{2S}{R_H}, \quad (31)$$

where p_v is vapor pressure and polytropic index, κ , is set to be 1 in order that the bubble temperature finally be back to T_0 . For adiabatic bubbles, κ needs to be replaced with γ_g . Given p_{lH} , equation (31) determines the corresponding equilibrium radius, R_H . From equations (28) and (30),

$$n_H = n_0 \left[(1 - \alpha_0) \left(\frac{p_{l0} + B}{p_{lH} + B} \right)^{\frac{1}{\gamma}} + \frac{4\pi}{3} n_0 \overline{R}_H^3 \right]^{-1}, \quad (32)$$

so that the far downstream void fraction is computed by $\alpha_H = (4\pi/3)n_H \overline{R}_H^3$. From equations (28) and (29), we find the steady shock speed,

$$U_s = \sqrt{\frac{p_{lH} - p_{l0}}{\rho_0 \left(1 - \frac{\rho_0}{\rho_H} \right)}}. \quad (33)$$

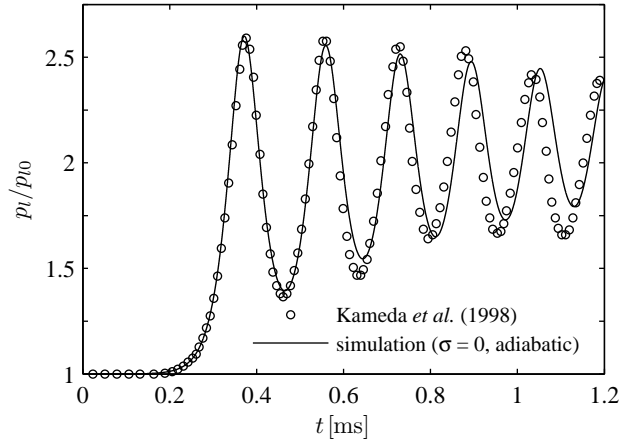


Figure 4. Comparison between the experiment of Kameda et al. [19] and simulation. The figure shows time history of liquid pressure for shock propagation in an $\text{SF}_6/\text{silicone-oil}$ ($\gamma = 10.0$, $B = 92.4 \text{ MPa}$) monodisperse mixture of $\alpha_0 = 0.24\%$ and $R_0^{\text{ref}} = 0.613 \text{ mm}$.

The induced velocity far downstream of the shock is then given by

$$u_H = u'_H + U_s = \left(1 - \frac{\rho_0}{\rho_H} \right) U_s. \quad (34)$$

The steady shock relations derived here are similar to those of Matsumoto and Kameda [17].

For shocks of infinitesimal strength, $\Delta p_l = p_{lH} - p_{l0} \ll p_{l0}$, the shock speed (33) reduces to the sonic speed (14). That is,

$$U_s = c + O(\Delta p_l). \quad (35)$$

This implies that the shock Mach number can formally be defined as $M_s = U_s/c$, which satisfies that $M_s \rightarrow 1$ as $\Delta p_l \rightarrow 0$.

Comparison to experiment

To validate the continuum model, we simulate the experiment of Kameda et al. [19] in which a spatially uniform bubble distribution was carefully created. In the computation, the steady shock relations discussed in the previous section are initially imposed by a diaphragm at $x = 0$.

We now compute shock propagation ($p_{lH} = 2.157 p_{l0}$) in an $\text{SF}_6/\text{silicone-oil}$ monodisperse mixture of $\alpha_0 = 0.24\%$. The equilibrium bubble radius is 0.613 mm (the corresponding Peclet number, $\text{Pe} = 3770$). Following equation (23), the large value of Pe means that the thermal boundary layer is thin compared to the bubble radius. The bubbles thus tend to behave adiabatically; the adiabatic relation with $\kappa = \gamma_g = 1.09$, rather than equation (13),

is employed in the computation. Given the shock strength and the adiabatic assumption, $M_s = 1.41$. The physical properties are found in [19].

The comparison is made in figure 4 showing the time history of the liquid pressure at $x = 1.462$ m. The simulation well reproduces the amplitude and phase of the relaxation oscillations. This agreement validates the capability of the continuum model (1) to (3) in resolving weak shock structures in monodisperse mixtures.

Before concluding this section, we check the continuum model limitations in figure 4. The oscillation period, τ , is 0.18 ms, so that the wavelength associated with the relaxation oscillations is approximately $U_s\tau = 5.7$ cm. The mean bubble spacing is computed by

$$l = \sqrt[3]{\frac{4\pi}{3\alpha_0}} R_0^{\text{ref}} = 12R_0^{\text{ref}} = 7.4 \text{ mm.} \quad (36)$$

It is therefore concluded that the continuum model is accurate since these length scales satisfy the continuum assumptions (b) and (c).

Steady shock structure

As discussed in figures 2 and 3, the bubble size distribution is found to increase the attenuation of the linear wave propagation for the low-frequency range. Here, the effect of the bubble statistics on the structure of shocks propagating in polydisperse mixtures is examined.

We compute shock propagation ($p_{IH} = 2p_{I0}$) in an air/water mixture of $\alpha_0 = 0.5\%$ at STP. The bubble size is assumed lognormally distributed about $R_0^{\text{ref}} = 10 \mu\text{m}$ with standard deviation, σ , ranging from 0 to 0.7. For 10- μm air/water-vapor bubbles at STP, $\text{Pe} = 9.87$. Given the shock strength and the isothermal assumption with $\kappa = 1$ in equation (31), the corresponding shock Mach number is computed as $M_s \approx 1.4$ for all σ . We judge steady shock propagation by observing the first peak of the relaxation oscillations; if the peak pressure is unchanged, the shock propagation can be considered to be in a steady state.

Figure 5 shows the liquid pressure and void fraction distributions for the steady shock propagation. The position where the liquid pressure is $(p_{I0} + p_{IH})/2$ is set at $x = 0$. For the monodisperse case ($\sigma = 0$), the relaxation oscillations appear behind the leading shock as observed in the experiments [13, 15, 18, 19]. As seen in the linear, low-frequency waves in figure 2, the wave structure becomes less oscillatory and the first peak becomes less steep by broadening the bubble size distribution. In other words, the bubble statistics associated with the size distribution yield an “apparent” damping mechanism of the shock dynamics. Because the different-sized bubbles oscillate with different frequencies as in the linear case, phase cancellations in a polydisperse bubble cloud occur locally and the polydisperse cloud does not oscillate in volume (or in void fraction) at the statistical equilibrium

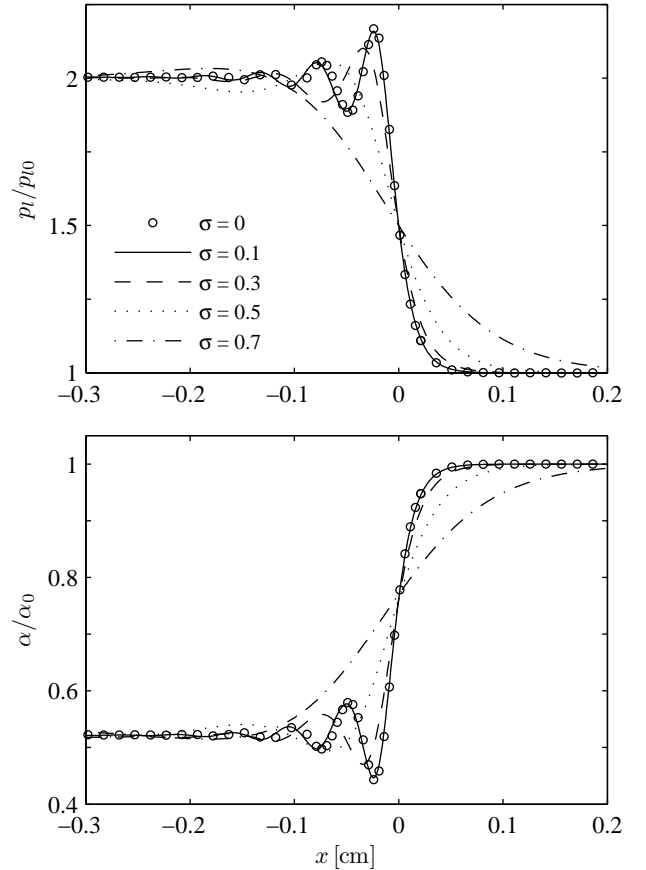


Figure 5. Liquid pressure (top) and void fraction (bottom) distributions for steady shock propagation in an air/water mixture of $\alpha_0 = 0.5\%$ and $R_0^{\text{ref}} = 10 \mu\text{m}$.

in a one-way-coupling sense. This cloud effect thus leads to the apparent damping to make the shock structure less oscillatory. If the distribution is sufficiently broad ($\sigma = 0.7$), the shock profile is practically monotonic; the polydisperse bubble cloud with $\sigma = 0.7$ can be regarded to behave quasistatically. The smooth shock profile in a polydisperse mixture was experimentally identified by Beylich and GÜLHAN [15].

Finally, we check the continuum model limitations. For the lognormal size distributions, the mean bubble spacing is computed by

$$l = \sqrt[3]{\frac{4\pi}{3\alpha_0}} \exp\left(\frac{3\sigma^2}{2}\right) R_0^{\text{ref}}. \quad (37)$$

For $\sigma = 0.7$, $l \approx 20R_0^{\text{ref}} = 0.2 \text{ mm}$, which is much shorter than the wavelength of the smooth shock profile in figure 5; therefore, assumption (c) is adequately satisfied. There may be an issue with

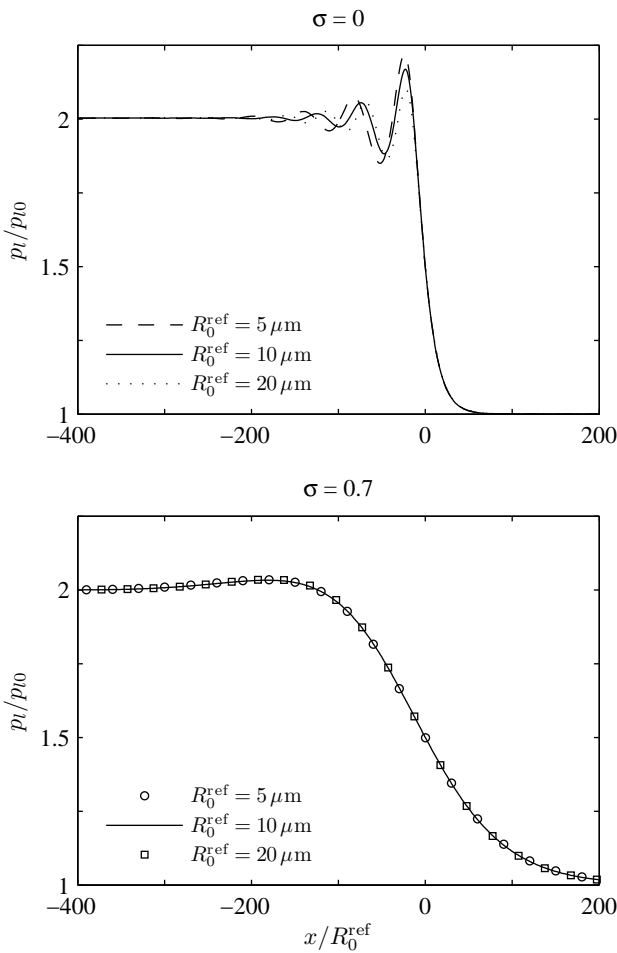


Figure 6. Effect of probable bubble size, R_0^{ref} , on steady shocks propagating in an air/water mixture of $\alpha_0 = 0.5\%$. $M_s \approx 1.4$ for all cases.

the interactions between the largest bubbles, but this is difficult to assess.

Effects of other parameters

We further conduct parameter studies of probable bubble size, R_0^{ref} , initial void fraction, α_0 , and shock strength, p_{IH} , and investigate the effects of these parameters on the steady shock structure. In all the examples presented here, we also discuss the effects of polydispersity by using the lognormal size distribution with $\sigma = 0$ (monodisperse) and $\sigma = 0.7$ (polydisperse).

The effect of probable bubble size, R_0^{ref} , is examined in figure 6. This plot shows the liquid pressure distribution for steady shocks ($p_{IH} = 2p_{l0}$) propagating in an air/water mixture of $\alpha_0 = 0.5\%$. We consider three probable bubble sizes ($5\mu\text{m}$, $10\mu\text{m}$, $20\mu\text{m}$) in the lognormal distribution. The corresponding Peclet numbers for the air/water-vapor bubbles are (5.79, 9.87,

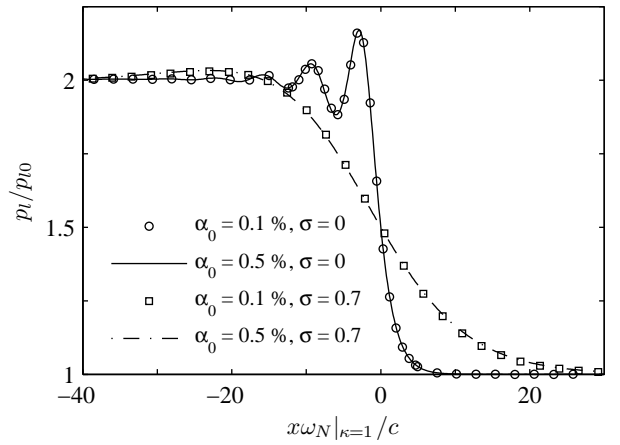


Figure 7. Effect of initial void fraction, α_0 , on steady shocks propagating in an air/water mixture of $R_0^{\text{ref}} = 10\mu\text{m}$. $M_s \approx 1.4$ for all cases.

18.1), respectively. The spatial coordinate (x -axis) is normalized by R_0^{ref} . It follows from the monodisperse cases that the first peak decreases as the bubble size increases; the thermal behavior of the bubbles represented by the Peclet number is critical to the shock structure in the monodisperse mixtures. However, the inclusion of the broad size distribution with $\sigma = 0.7$ leads to the fact that the shock profiles coincide in the normalized coordinate. In other words, the dynamics of the polydisperse bubble cloud are insensitive to the single bubble dynamics, which are unimportant at the statistical equilibrium in the one-way-coupling problem. We may therefore say that the effect of polydispersity dominates over the physical damping associated with the single bubble dynamics if the size distribution is sufficiently broad.

Next, we examine the effect of void fraction, α_0 , in figure 7. This plot shows the liquid pressure distribution for steady shocks ($p_{IH} = 2p_{l0}$) propagating in an air/water mixture of $R_0^{\text{ref}} = 10\mu\text{m}$. We consider two initial void fractions (0.1%, 0.5%). The corresponding sonic speeds (14) in the unperturbed states are (312 m/s, 142 m/s), respectively. In the normalized spatial coordinate ($x\omega_N|_{\kappa=1}/c$), the shock profiles coincide for both monodisperse and polydisperse cases. That is, the void fraction simply changes the propagation speed, but the shock profile remains similar.

Last, we study the effect of shock strength, p_{IH} , in figure 8. This plot shows the liquid pressure distribution for steady shocks propagating in an air/water mixture of $\alpha_0 = 0.5\%$ and $R_0^{\text{ref}} = 10\mu\text{m}$. We consider two shock strengths ($2p_{l0}$, $3p_{l0}$). In the monodisperse case, the stronger shock results in the larger amplitude of the relaxation oscillations. As in the previous examples, the lognormal size distribution with $\sigma = 0.7$ smooths the oscillatory shock structure. Note that the overshoot in the smooth structure becomes larger as the shock pressure increases.

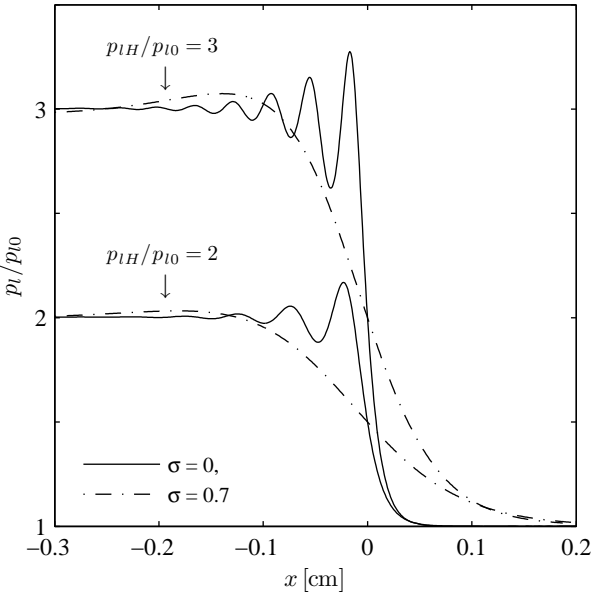


Figure 8. Effect of shock strength, p_{IH} , on steady shocks propagating in an air/water mixture of $\alpha_0 = 0.5\%$ and $R_0^{\text{ref}} = 10\mu\text{m}$. $M_s \approx 1.4$ for $p_{IH} = 2p_{l0}$ and $M_s \approx 1.7$ for $p_{IH} = 3p_{l0}$.

BUBBLE SCREEN PROBLEMS

Bubble screens are a useful problem in understanding the fundamental physics of shock/bubble-cloud interactions and are used to prevent damage of submerged structures due to underwater explosions [51]. Reflection and transmission of linear waves propagating through a bubble screen were formulated in [37,38].

To understand nonlinear wave interactions in bubble screens, we solve shock propagation through a one-dimensional air-bubble screen in water:

$$\alpha = \begin{cases} \alpha_0, & \text{if } 0 < x/h < 1; \\ \varepsilon, & \text{otherwise.} \end{cases} \quad (38)$$

where $0 < \varepsilon \ll \alpha_0 = 0.5\%$ and $h = 2\text{cm}$ (width of the screen). The bubble size in the screen is assumed lognormally distributed about $R_0^{\text{ref}} = 50\mu\text{m}$ with $\sigma = 0$ (monodisperse) and $\sigma = 0.7$ (polydisperse). For $50\mu\text{m}$ air/water-vapor bubbles at STP, $\text{Pe} = 42.8$. The incident (right-going) shock of strength, $p_{IH} = 5p_{l0}$, is initially placed at $x < 0$. The corresponding shock Mach number (defined in pure water domain) is $M_s = 1.0004$, so that the shock speed is very close to the sonic speed. The transmitted wave is measured at $x = 2.12\text{cm}$.

The snapshots of the liquid pressure distribution are shown in figure 9. At the left interface ($x = 0$), the incident shock reflects as a rarefaction wave and transmits as a shock due to the fact

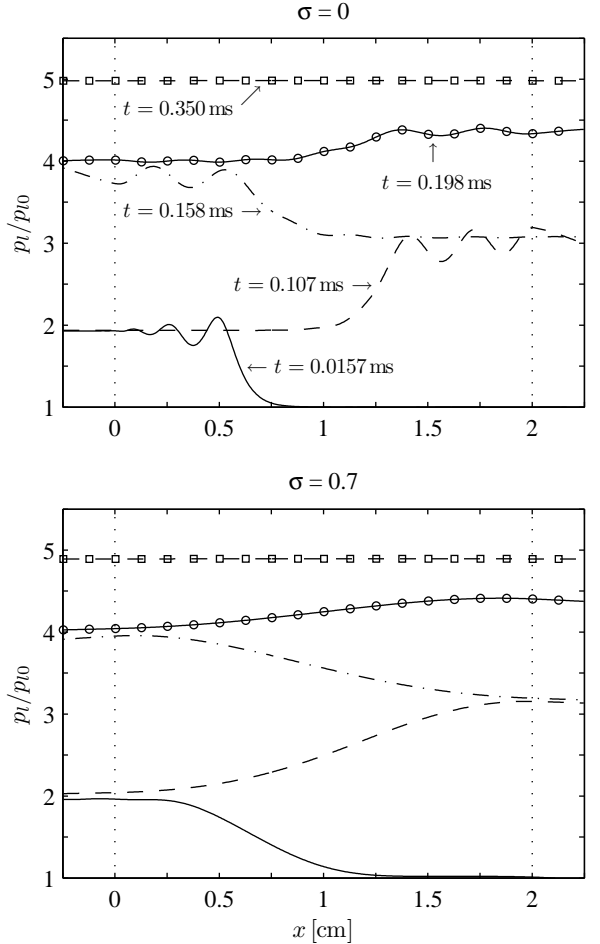


Figure 9. Liquid pressure distribution for shock propagation through an air/water bubble screen of $\alpha_0 = 0.5\%$ and $R_0^{\text{ref}} = 50\mu\text{m}$. The bubble screen is initially placed between dotted lines. At $t = 0$, the precursory wave reaches at a probe ($x = 2.12\text{cm}$).

that the acoustic impedance of the screen is smaller than that of water (i.e. $\rho_c < \rho_l c_l$). The transmitted shock (trapped in the screen) keeps reflecting at the interfaces and the pressure inside the screen eventually increases to the incident shock pressure. We notice that the size distribution smooths out the oscillatory structure of the trapped waves as seen in figure 5.

The pressure just downstream of the bubble screen is presented in figure 10. At $t = 0$, the precursory waves propagating with the sonic speed of water are measured. Note that for the case of no bubble screen, the probe pressure would show an instantaneous jump to p_{IH} at $t \approx 0$. The bubble size distribution with $\sigma = 0.7$ increases the amplitude of the precursors because the size distribution decreases attenuation of the wave propagation (see figure 3). The transmitted waves leave the screen at late times, and the liquid pressure increases in a step-wise manner

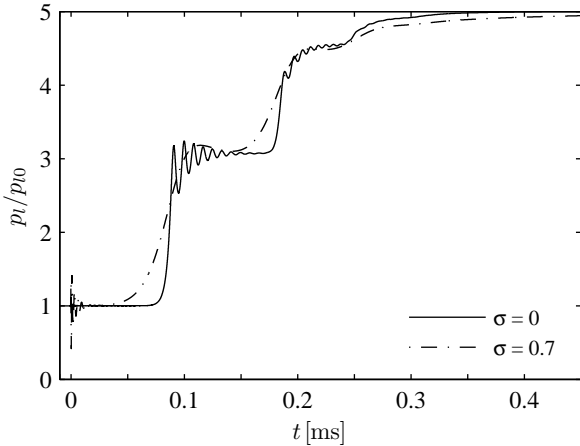


Figure 10. Time history of liquid pressure for the transmitted waves as they leave the bubble screen in figure 9.

because of the reflections of the trapped waves in the screen. As expected, the size distribution makes the pressure evolution less oscillatory and broaden the shock width. Hence, the size distribution may be capable of cushioning impulsive loading due to underwater explosions.

CONCLUSION

The continuum bubbly flow model including the effect of distributed bubble sizes is formulated and the numerical scheme has been shown to be capable of simulating wave phenomena in polydisperse mixtures. The bubble size distribution is found to lead to apparent damping of the shock dynamics due to phase cancellations among the different-sized bubbles and make the wave structure less oscillatory. If the size distribution is sufficiently broad, the effect of polydispersity dominates over the physical damping associated with the single bubble dynamics and the shock profile is smoothed out. The bubble screen computations indicate that the size distribution in the screen has potential for cushioning impulsive loading due to underwater explosions.

ACKNOWLEDGMENT

This work was supported by ONR Grant N00014-06-1-0730 and by NIH Grant PO1 DK043881.

REFERENCES

- [1] Cole, R. H., 1948. *Underwater Explosions*. Princeton University Press.
- [2] Wardlaw, A. B., and Luton, J. A., 2000. "Fluid-structure in-

teraction mechanisms for close-in explosions". *Shock Vibr.*, **7**, 265–275.

- [3] Futakawa, M., Naoe, T., Tsai, C. C., Kogawa, H., Ishikura, S., Ikeda, Y., Soyama, H., and Date, H., 2003. "Cavitation erosion in mercury target of spallation neutron source". In Proceedings of the Fifth International Symposium on Cavitation, Osaka, Japan.
- [4] Futakawa, M., Kogawa, H., Hasegawa, S., Ikeda, Y., Riemer, B., Wendel, M., Haines, J., Bauer, G., Naoe, T., Tanaka, N., Okita, K., Fujiwara, A., and Matsumoto, Y., 2006. "Cavitation erosion by proton beam bombarding mercury target for neutron spallation source (Damage potential evaluation by measuring acoustic vibration)". In Proceedings of the Sixth International Symposium on Cavitation, Wageningen, The Netherlands.
- [5] Arndt, R. E. A., 1981. "Cavitation in fluid machinery and hydraulic structures". *Ann. Rev. Fluid Mech.*, **13**, 273–328.
- [6] Brennen, C. E., 1994. *Hydrodynamics of Pumps*. Oxford University Press.
- [7] Brennen, C. E., 1995. *Cavitation and Bubble Dynamics*. Oxford University Press.
- [8] Bailey, M. R., Evan, A. P., Sapozhnikov, O. A., Cleveland, R. O., and Colonius, T., 2003. "Cavitation in shock wave lithotripsy". In Proceedings of the Fifth International Symposium on Cavitation, Osaka, Japan.
- [9] Tanguay, M., and Colonius, T., 2003. "Progress in modeling and simulation of shock wave lithotripsy (SWL)". In Proceedings of the Fifth International Symposium on Cavitation, Osaka, Japan.
- [10] Takayama, K., 2004. "Shock wave/geophysical and medical applications". *Ann. Rev. Fluid Mech.*, **36**, 347–379.
- [11] Campbell, I. J., and Pitcher, A. S., 1958. "Shock waves in a liquid containing gas bubbles". *Proc. R. Soc. Lond. A*, **243**, 534–545.
- [12] Nigmatulin, R. I., and Shagapov, V. S., 1974. "Structure of shock waves in a liquid containing gas bubbles". *Fluid Dyn.*, **9**, 890–899.
- [13] Noordzij, L., and van Wijngaarden, L., 1974. "Relaxation effects, caused by relative motion, on shock waves in gas-bubble/liquid mixtures". *J. Fluid Mech.*, **66**, 115–143.
- [14] Nigmatulin, R. I., 1982. "Mathematical modelling of bubbly liquid motion and hydrodynamical effects in wave propagation phenomenon". *Appl. Sci. Res.*, **38**, 267–289.
- [15] Beylich, A. E., and Gühan, A., 1990. "On the structure of nonlinear waves in liquids with gas bubbles". *Phys. Fluids A*, **2**, 1412–1428.
- [16] Watanabe, M., and Prosperetti, A., 1994. "Shock waves in dilute bubbly liquids". *J. Fluid Mech.*, **274**, 349–381.
- [17] Matsumoto, Y., and Kameda, M., 1996. "Propagation of shock waves in dilute bubbly liquids (Governing equations, Hugoniot relations, and effect of slippage between two phases)". *JSME Int. J. Ser. B*, **39**, 246–272.

- [18] Kameda, M., and Matsumoto, Y., 1996. "Shock waves in a liquid containing small gas bubbles". *Phys. Fluids*, **8**, 322–335.
- [19] Kameda, M., Shimaoka, N., Higashino, F., and Matsumoto, Y., 1998. "Shock waves in a uniform bubbly flow". *Phys. Fluids*, **10**, 2661–2668.
- [20] Zhang, Z. D., and Prosperetti, A., 1994. "Ensemble-averaged equations for bubbly flows". *Phys. Fluids*, **6**, 2956–2970.
- [21] Zhang, Z. D., and Prosperetti, A., 1997. "Momentum and energy equations for disperse two-phase flows and their closure for dilute suspensions". *Int. J. Multiphase Flow*, **23**, 425–453.
- [22] d'Agostino, L., Brennen, C. E., and Acosta, A. J., 1988. "Linearized dynamics of two-dimensional bubbly and cavitating flows over slender surfaces". *J. Fluid Mech.*, **199**, 485–509.
- [23] Prosperetti, A., and Lezzi, A., 1986. "Bubble dynamics in a compressible liquid (Part 1. First-order theory)". *J. Fluid Mech.*, **168**, 457–478.
- [24] Thompson, P. A., 1972. *Compressible-Fluid Dynamics*. McGraw-Hill.
- [25] Tanguay, M., 2004. "Computation of bubbly cavitating flow in shock wave lithotripsy". PhD Thesis, Calif. Inst. of Tech., Pasadena, CA.
- [26] van Wijngaarden, L., 1972. "One-dimensional flow of liquids containing small gas bubbles". *Ann. Rev. Fluid Mech.*, **4**, 369–396.
- [27] Katz, J., 1978. Determination of solid nuclei and bubble distributions in water by holography. Eng. and Appl. Sci. Dev. Rep. 183-3, Calif. Inst. of Tech.
- [28] O'Hern, T. J., d'Agostino, L., and Acosta, A. J., 1988. "Comparison of holographic and Coulter Counter measurements of cavitation nuclei in the ocean". *J. Fluids Eng.*, **110**, 200–207.
- [29] Prosperetti, A., Crum, L. A., and Commander, K. W., 1988. "Nonlinear bubble dynamics". *J. Acoust. Soc. Am.*, **83**, 502–514.
- [30] Preston, A. T., Colonius, T., and Brennen, C. E., 2007. "A reduced-order model of diffusive effects on the dynamics of bubbles". *Phys. Fluids*, **19**, 123302.
- [31] Plesset, M. S., and Prosperetti, A., 1977. "Bubble dynamics and cavitation". *Ann. Rev. Fluid Mech.*, **9**, 145–185.
- [32] Fujikawa, S., and Akamatsu, T., 1980. "Effects of the non-equilibrium condensation of vapour on the pressure wave produced by the collapse of a bubble in a liquid". *J. Fluid Mech.*, **97**, 481–512.
- [33] Gilmore, F. R., 1952. The collapse and growth of a spherical bubble in a viscous compressible liquid. Hydrodynamic Lab. Rep. 26-4, Calif. Inst. of Tech.
- [34] Nigmatulin, R. I., Khabelev, N. S., and Nagiev, F. B., 1981. "Dynamics, heat and mass transfer of vapour-gas bubbles in a liquid". *Int. J. Heat Mass Transfer*, **24**, 1033–1044.
- [35] Colonius, T., Hagmeijer, R., Ando, K., and Brennen, C. E., 2008. "Statistical equilibrium of bubble oscillations in dilute bubbly flows". *Phys. Fluids*, **20**, 040902.
- [36] Brennen, C. E., 2002. "Fission of collapsing cavitation bubbles". *J. Fluid Mech.*, **472**, 153–166.
- [37] Carstensen, E. L., and Foldy, L. L., 1947. "Propagation of sound through a liquid containing bubbles". *J. Acoust. Soc. Am.*, **19**, 481–501.
- [38] Commander, K. W., and Prosperetti, A., 1989. "Linear pressure waves in bubbly liquids: Comparison between theory and experiments". *J. Acoust. Soc. Am.*, **85**, 732–746.
- [39] Waterman, P. C., and Truell, R., 1961. "Multiple scattering of waves". *J. Math. Phys.*, **2**, 512–537.
- [40] Feuillaude, C., 1996. "The attenuation and dispersion of sound in water containing multiply interacting air bubbles". *J. Acoust. Soc. Am.*, **99**, 3412–3430.
- [41] Shu, C. W., and Osher, S., 1988. "Efficient implementation of essentially non-oscillatory shock-capturing schemes". *J. Comput. Phys.*, **77**, 439–471.
- [42] Liu, X. D., Osher, S., and Chen, T., 1994. "Weighted essentially non-oscillatory schemes". *J. Comput. Phys.*, **115**, 200–212.
- [43] Toro, E. F., Spruce, M., and Speares, W., 1994. "Restoration of the contact surface in the HLL-Riemann solver". *Shock Waves*, **4**, 25–34.
- [44] Thompson, K. W., 1987. "Time dependent boundary conditions for hyperbolic systems". *J. Comput. Phys.*, **68**, 1–24.
- [45] Prosperetti, A., 1977. "Thermal effects and damping mechanisms in the forced radial oscillations of gas bubbles in liquids". *J. Acoust. Soc. Am.*, **61**, 17–27.
- [46] Prosperetti, A., 1991. "The thermal behaviour of oscillating gas bubbles". *J. Fluid Mech.*, **222**, 587–616.
- [47] Lide, D. R., ed., 2006. *CRC Handbook of Chemistry and Physics*, 87th ed. CRC Press, ch. 6.
- [48] Kuznetsov, V. V., Nakoryakov, V. E., Pokusaev, B. G., and Shreiber, I. R., 1978. "Propagation of perturbations in a gas-liquid mixture". *J. Fluid Mech.*, **85**, 85–96.
- [49] Smereka, P., 2002. "A Vlasov equation for pressure wave propagation in bubbly fluids". *J. Fluid Mech.*, **454**, 287–325.
- [50] Ando, K., Colonius, T., and Brennen, C. E., 2009. "Improvement of acoustic theory of ultrasonic waves in dilute bubbly liquids". *J. Acoust. Soc. Am.*, In press.
- [51] Domenico, S. N., 1982. "Acoustic wave propagation in air-bubble curtains in water (Part 1: History and theory)". *Geophysics*, **47**, 345–353.